

Strain-induced tuning of optical properties of layered MoS_2

Shubham Bhagat^a, Shivani Sharma^a, Jasvir Singh^a, Sandeep Sharma^{a,*}

^a*Department of Physics, Guru Nanak Dev University, Amritsar 143005, India*

Abstract

The sensitive correlation between optical parameters and strain in MoS_2 results in a totally different approach to tune the optical properties. Usually, an external source of strain is employed to monitor the optical and vibrational properties of a material. It is always challenging to have a precise control over the strain and its consequences on material properties. Here, we report the presence of a compressive strain in MoS_2 crystalline powder and nanosheets obtained via the process of ball-milling and probe sonication. The diffraction peaks in the X-ray diffraction pattern shift to higher 2θ value implying a compressive strain that increases with the processing time. The absorption spectra, photoluminescence and Raman modes are blue-shifted w.r.t the bulk unprocessed sample. The observed blue-shift is attributed to the presence of compressive strain in the samples. Whereas in thin nano sheets of MoS_2 , it is very likely that both quantum confinement as well as strain result in the observed blue-shift. These results indicate that by optimizing the processing conditions and/or time, a strain of desired amount and hence tunable shift in optical properties of material can be achieved.

Keywords: MoS_2 , Excitonic absorption, Photoluminescence, 2-D Transition-metal dichalcogenides

*Corresponding author

Email address: shubh.279@gmail.com (Shubham Bhagat)

Introduction

The transition-metal di-chalcogenides (TMDCs) of the type MX_2 (where $M = \text{Mo, W}$ and $X = \text{S, Se etc}$) are an exciting class of 2-dimensional (2-D) materials which possess intriguing optical, electrical and thermal properties A R Beal (1976); Wang et al. (2012); Kin Fai Mak (2016). In bulk form they exhibit an indirect band gap ($\approx 1.2\text{eV}$) and a direct band gap ($\approx 1.8\text{ eV}$) when reduced to a monolayer. Their non-zero direct band gap is larger than silicon (1.12 eV) and considerable smaller amount of off-state leakage current is expected in devices prepared on TMDCs monolayers. Further, the direct band gap values of these materials lies in the visible region of the spectrum and therefore, these 2-D materials are promising for nanoelectronics and optoelectronics devices Wang et al. (2012); Kin Fai Mak (2016). Although, graphene with exceptionally large mobility ($\approx 10^5\text{cm}^2\text{V}^{-1}\text{s}^{-1}$) Allen et al. (2010); Choi et al. (2010); was the first 2-D material that has been extensively studied, the lack of band gap make it unsuitable for many optical and electronics applications. Due to their ultrathin nature, a most common feature shared by these 2-D materials is that they are quite sensitive to external perturbations such as strain. Whereas the effect of strain on electronic, optical and vibrational properties of graphene is extensively studied Ni et al. (2008); Castro Neto et al. (2009); Huang et al. (2010); Novoselov (2011), the theoretically predicted band-gap opening by external strain has still remained elusive Lee et al. (2008); Kim et al. (2009); Therefore limiting the use of graphene in digital devices. On the other hand, 2-D TMDCs like MoS_2 are predicted to have highly strain-tunable optical and electronic properties Wang et al. (2012); Lu et al. (2012). Not only limited to these areas, the strained nanostructures of MoS_2 have also been predicted to possess improved electrical conductivity and a large value of thermopower (250-350 $\mu\text{V}/\text{K}$) Bhattacharyya et al. (2014).

Thus, the strain has significant influence on electronic, optical as well as thermoelectric properties of the material. Different methods for inducing strain on 2-D materials have been developed. For instance He et.al. studied the response

of MoS_2 under uniaxial tensile strain by using a cantilever device. They observed a red-shift in band gap and photoluminescence emission spectra of MoS_2 He et al. (2013a). On the other hand, Hui et.al have used an electromechanical device to apply a uniform and controllable compressive strain in trilayer MoS_2 Hui et al. (2013). They reported a blue-shift in optical as well as in vibrational spectra of the compressed MoS_2 thin layers. Thus, a tensile and compressive strain give rise to a red-shift and blue-shift, respectively.

Here, we report a different approach to introduce strain in the samples during the synthesis process. We prepared samples using ball-milling followed by probe sonication. During the ball-milling zirconium balls apply shear and compression forces on the powdered sample, resulting in exfoliation of multi-layered sample. This process can result in a compressive strain in the layered material. We have observed a negative compressive strain giving rise to a blue-shift in optical properties. These results are in agreement with previously reported experimental and theoretical data.

Experimental

Initially, 2 gm of powder was mixed with isopropyl alcohol. Thereafter, the mixture was processed using high energy ball milling for 32 hours. The grinded sample was dried in oven at 80°C . From the dried sample, 1 gm was kept aside and named S1. The remaining sample was mixed with Dimethylformamide (DMF) and processed with a probe sonicator (750 Watt, 20 kHz, PCI-Analytics, India). After probe sonication, suspension obtained was centrifuged at 10,000 rpm for 20 minutes. Thin sheets floating on the surface of suspension were noticed. The sheets were transferred to the glass slide using dip coating method. The remaining sample was dried to obtain the powder. This powder sample so obtained was named S2. The sample prepared by dip coating was named S3. All the structural and optical characterizations were done on the samples S1, S2 and S3.

For the structural analysis, X-ray diffraction (XRD), Scanning electron mi-

croscope (SEM) and high resolution transmission electron microscope (HRTEM) were used. XRD patterns were obtained using Shimadzu 7000 X-Ray Diffractometer ($\text{Cu } K_\alpha$ radiation). High resolution Transmission electron microscopic images were obtained using JEOL (JEM-2100). Optical absorption spectra of the samples was obtained by using Shimadzu UV-Vis 2450 spectrophotometer and photoluminescence emission spectra was recorded using Perkin Elmer LS55 fluorescence Spectrometer. The vibrational modes in synthesized samples were studied using Renishaw Invia Reflex micro Raman spectrometer using excitation wavelength of 514 nm.

Results and Discussion

X-Ray Diffraction

Fig.1 compares the diffraction pattern obtained from bulk material, samples S1, S2 and S3. The bulk sample shows various diffraction peaks belonging to different planes of highly crystalline MoS_2 . All diffraction peaks can be indexed with crystalline structure (JCPDS 77-1716, P63/ mmc space group, H- MoS_2). It is clear from the data that all samples display intense (002) peak and other peaks of relatively lower intensity. This, confirms the layered structure of the material giving rise to dominant exposure of the (002) planes in all samples. We observe that samples S1, S2 and bulk MoS_2 , contain a large number of peaks in the diffraction spectra, whereas sample S3 consists of three peaks belonging to (002), (006) and (112) planes. Intense (002) peak indicates the highly layered structure of the deposited nanosheets.

A close analysis of the data reveals [inset in Fig.1] that all peaks in sample S1 and S2 have shifted towards higher θ values. This implies that after ball milling and probe-sonication a uniform stress within the sample give rise to a uniform strain. This uniform strain causes a line shift in the peak position. This shift causes a lower d value for the planes. Thus, we can calculate the uniform strain or the macrostrain by comparing the experimentally determined ' d_{exp} ' values with the reference values from JCPDS data for the bulk. The macrostrain is

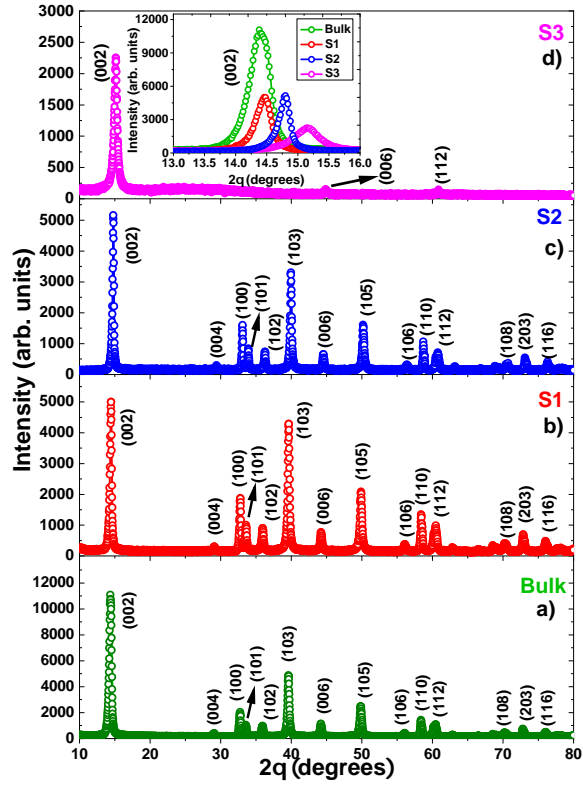


Figure 1: (color online) X-ray diffraction pattern from (a) bulk crystalline MoS_2 powder, Sample (b) S1 (c) S2 and (d) S3, thin sheets of MoS_2

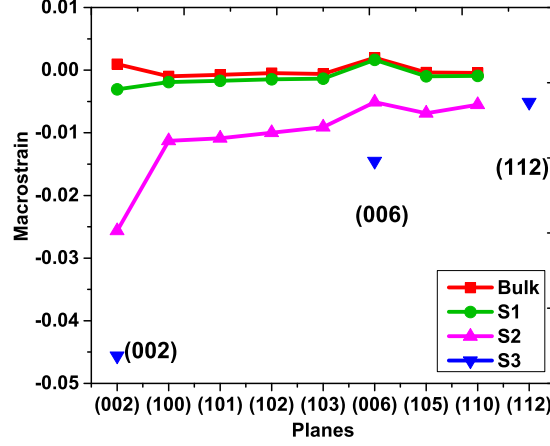


Figure 2: (color online) Variation of macrostrain for different samples

estimated using the relation:

$$macrostrain = \frac{d_{exp} - d_{ref}}{d_{ref}} \quad (1)$$

where interplanar distance $d_{exp} = \lambda/2 \sin \theta$ and d_{ref} is the respective value in JCPDS data Sinha et al. (2012). Strain calculations were performed for all peaks and data is shown in Fig.2. It is inferred that bulk crystalline powder display minor positive strain for (002)(0.09%) plane and negligible negative strain for all other planes. Rest of the samples display a negative compressive strain, which is larger for planes with smaller indices. In sample S3, we observed only three peaks and corresponding compressive strain is larger than other samples. For (002) plane the absolute value is around 4.56%, quite larger from S1 and S2. Thus, we see that processes of ball-milling and probe sonication give rise to a strain in the sample.

Transmission Electron Microscopy

Fig.3(a) and (b) show the low resolution transmission electron microscopic (TEM) image of ball milled sample. (c) and (d) are the similar images for sample S2. As we see, the ball-milling has reduced the size significantly from

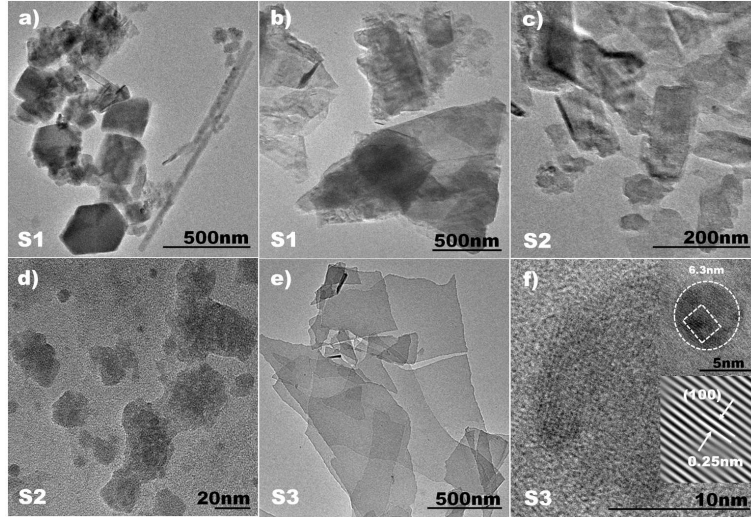


Figure 3: (color online) (a) and (b) Low resolution TEM-images of sample S1, (c) and (d) sample S2, (e) sample S3 and (f) HR-TEM image of sample S3. Note that in sample S3 ultra thin sheets together with particles of smaller size are obtained

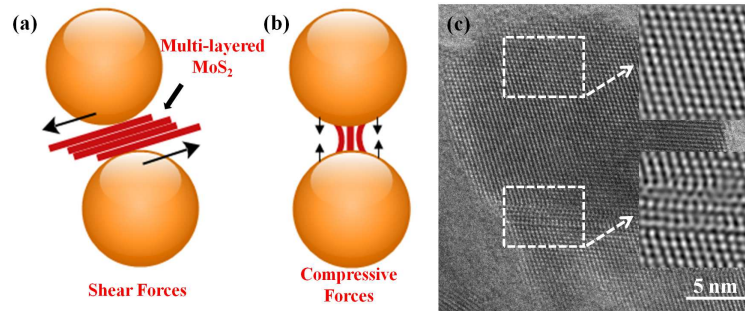


Figure 4: (color online) Fig. (a) and (b) give a representation of shear and compressive forces acting on the sample during ball milling. In (c) HR-TEM image of a thick sheet obtained after ball milling is shown. For more details, refer to the text.

μ m to a few hundred of nano meters. Particle sizes of various dimensions are obtained. A significant difference is seen in sample S3, where ultra thin nanosheets together with particles of sub-nanometer sizes are obtained. The upper inset in (f) shows the HR-TEM image of a particle and lower inset displays the fast fourier transformed image of the area shown in upper inset. The lattice fringes with spacing of 0.25 nm corresponding to (100) can be clearly seen. The Fig.4 (a) and (b) display how the shear and compressive forces reduce the size of material during ball-milling. More important information is obtained from the HR-TEM image (c) of a thick sheet of MoS_2 . The upper inset in this image represents the digitally filtered image of the highlighted part. The hexagonal symmetry is clearly visible, and the lattice spacing is 0.35 nm. The lower inset represents the FFT image corresponding to lower part of the main image. Interesting features are visible from this image. As we see, the continuous running line are disrupted. This is indeed due to the compressive forces acting on the layered sample (Fig.4 (b)). This results in a compressive strain in the sample and as a result, the spacing between two adjacent (compressed) planes is ≈ 0.33 nm. These results corroborate the XRD data where, we have noticed that diffraction peaks have shifted towards higher θ values, thus suggesting the presence of a compressive strain in the samples.

Raman Spectroscopy

Fig.5 displays the typical Raman spectra of bulk, ball milled, probe sonicated sample and MoS_2 nanosheets. The spectra depicts the only two characteristic Raman active modes: A_{1g} and E_{2g}^1 which were obtained with excitation wavelength of 514 nm. Here, A_{1g} is the mode that arise due to out-of-plane motion of the Mo and S atoms. The E_{2g}^1 mode arises due to the in-plane motion of the Mo and S atoms Wang et al. (2012); Sharma et al. (2017) . In bulk sample, the in-plane mode E_{2g}^1 appears at 378.39 cm^{-1} , whereas the out-of-plane mode at 403.52 cm^{-1} . The separation between the two modes is 25.13 cm^{-1} , in good agreement with that found in mechanically exfoliated multilayered MoS_2 Plechinger et al. (2012). Both of these modes have shifted to

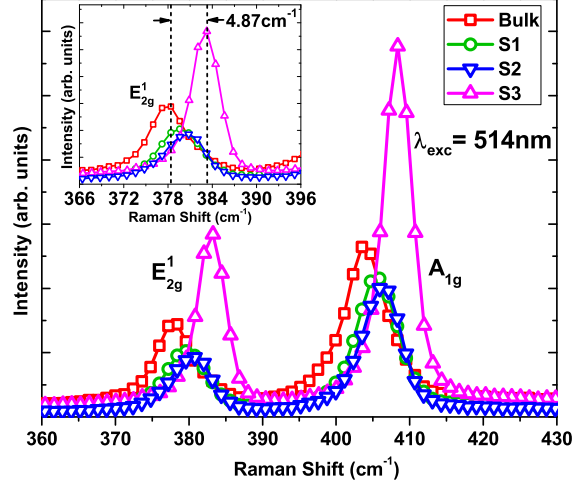


Figure 5: (color online) Comparison between raman spectra obtained from bulk crystalline powder, ball milled powder and thin sheets at 514 nm excitation wavelength. A blue-shift is clearly visible in the two modes.

higher frequencies in processed samples. In sample S1, the A_{1g} and E_{2g}^1 mode have shifted by 2.39 cm^{-1} and 1.19 cm^{-1} , respectively, with a shift ratio of A_{1g}^1/E_{2g}^1 of ≈ 1 . As we notice in the Table.1, the separation between these characteristics modes is almost similar in all samples. But, the sample S3 with nanosheets, has largest displacement w.r.t. the bulk sample. For e.g., the modes A_{1g} and E_{2g}^1 have shifted by 4.85 cm^{-1} and 4.87 cm^{-1} , respectively, with a shift ratio of ≈ 1 . Therefore, we notice that in ball-milled and probe sonicated samples the modes undergo a blue-shift. The sample with largest compressive strain shows largest blue-shift. Such a blue-shift in these two modes has previously been noticed in MoS_2 bulk crystals and nanotubes under high pressure and was attributed to the presence of compressive strain Hui et al. (2013); Bagnall et al. (1980); Virsek et al. (2007).

Table 1: Peak positions for characteristic Raman modes A_{1g} and E_{2g}^1 of MoS_2 in different samples at an excitation wavelength of 514nm. The last column gives the separation between these two modes.

Sample	A_{1g} (cm^{-1})	E_{2g}^1 (cm^{-1})	$A_{1g} - E_{2g}^1$ (cm^{-1})
Bulk	403.52	378.39	25.13
Ball-milled	405.91	379.58	26.33
Sonicated	405.92	380.8	25.12
Nanosheets	408.37	383.26	25.11

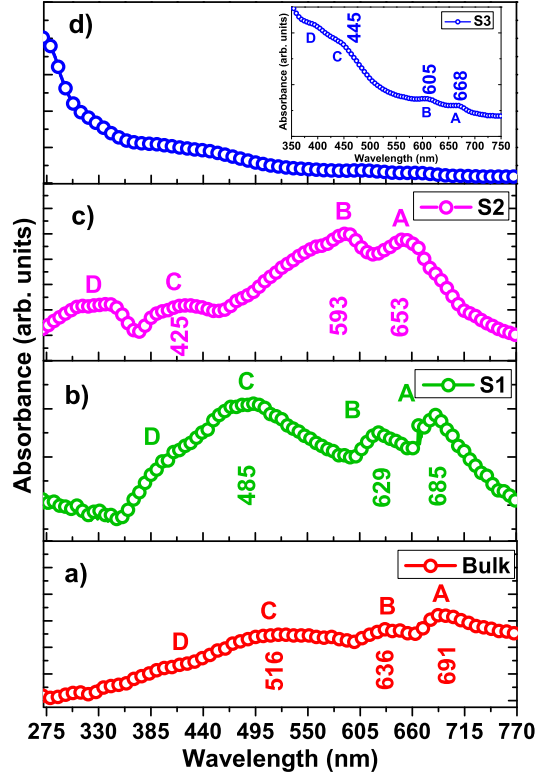


Figure 6: (color online) Absorption spectra of bulk MoS_2 and samples S1, S2 and S3.

UV-Vis Spectroscopy

Fig.6 compares the absorption spectra obtained from bulk crystalline MoS_2 , ball milled sample S1 and probe sonicated sample S2. The absorption spectra from nanosheets (S3) is also shown for comparison. The absorption spectra of the powder samples were obtained by using the diffuse reflectance geometry. Initially, the absorption coefficient was calculated using the Kubelka-Munk equation;

$$F(R) = \frac{(1 - R)^2}{R} = \frac{k}{s} \quad (2)$$

where, $F(R)$ is the Kubelka-Munk function (which is the required absorption coefficient α), R is the absolute reflectance of sample, k is the molar absorption coefficient and s is the scattering coefficient. The plot of $F(R)$ against wavelength gives the required absorption spectra Murphy (2007); Wood (1979); RosendoLpez (2012).

The absorption spectra for the bulk powder is shown in Fig6(a). The peaks marked as A (691 nm) and B (636 nm), are the characteristic excitonic peaks of MoS_2 . These peaks originate from transition between conduction band and spin-orbit-coupling (SOC) induced splitting of valence band energy levels. These peaks are separated by ≈ 156 meV, quiet close to the theoretically calculated value (160 meV) Mukherjee et al. (2015). However, it should be note that there exist a wider spread in the reported values of spin-orbit coupling strength in MoS_2 Bromley et al. (1972); Böker et al. (2001); Zhu et al. (2011); Trainer et al. (2017). For a single layer MoS_2 , splitting can entirely attributed to the SOC. However, in bulk it might be due to the combination of spin-orbit coupling and inter-layer coupling. But in literature, there is a disagreement between the relative strength of these two mechanism Klein et al. (2001); Jin et al. (2013); Molina-Sanchez et al. (2013); Alidoust et al. (2014); Suzuki et al. (2014); Eknapakul et al. (2014); Padilha et al. (2014); Latzke et al. (2015).

The other peaks marked as C and D are attributed to the direct transition from the depth of the valence band Wilcoxon & Samara (1995); Wilson & Yoffe (1969). The absorption spectrum from samples S1, S2 and S3 also display

Table 2: Summary of various peak positions in absorption spectra of different samples. Spin-orbit-coupling induced splitting between peak position A and B is also given for the comparison

Sample	A (nm)	B (nm)	A-B (meV)
Bulk	691	636	156
Ball-milled	685	629	162
Sonicated	653	593	190
Nanosheets	668	605	189

multiple spectral features that are blue-shifted w.r.t. the bulk. Therefore, after processing the different MoS_2 samples preserve the excitonic features and are blue-shifted. The maximum energy shift is close to ≈ 30 meV, comparatively much smaller than the value (≈ 780 meV) previously reported for MoS_2 nano clusters with sizes in the range of 4.5 nm Wilcoxon & Samara (1995); Wilcoxon et al. (1997). This was attributed to the phenomena of quantum confinement in the MoS_2 nanostructures Wilcoxon & Samara (1995); Gan et al. (2015). Another noticeable difference in sample S3 appears at lower wavelengths. Below 330 nm, the absorption rises and is attributed to the band edge absorption from scaled nanosheets of MoS_2 . It should be noted that quantum confinement effects come into picture when the particle size is close to the Bohr radius, 'R' which is different for different materials. The Bohr radius is expressed as

$$R = \epsilon \left(\frac{m_o}{\mu} \right) a_0 \quad (3)$$

where, ϵ is the dielectric constant of material in bulk form, m_0 is the free electron mass, reduced mass of the exciton $\mu = \frac{m_e \cdot m_h}{m_e + m_h}$, and $a_0 = 0.53 \text{\AA}$. For MoS_2 , the effective masses for electron and holes are; $m_e = 0.48m_0$, $m_h = 0.41m_0$ and $\epsilon = 11$ Mukherjee et al. (2015) and this gives $\mu \approx 0.22m_0$. As a result the exciton Bohr radius for MoS_2 is around 2.65 nm. Thus, when particle size is close to the Bohr radius, one can expect the enhancement in the band gap energy Gopalakrishnan et al. (2014) as well as increase in the excitonic absorption energy Wilcoxon & Samara (1995), thus giving a blue-shift in absorption ener-

gies. The indirect band gap for bulk MoS_2 is close to 1.23 eV and it changes to 1.89 eV when in monolayer form. Therefore, in sample S3, the band edge absorption close to 330 nm (3.8 eV) cannot be explained without invoking the quantum confinement phenomena in the nanosheets. Whereas, in samples S1 and S2 the particle size is quite far away from the quantum confinement regime, the observed blue-shift is indeed not due to confinement phenomena in the nanostructure. But, it is the presence of the compressive strain in these sample, which governs this blue-shift. Recently, He et.al. He et al. (2013a) has shown that applying a uniaxial tensile strain to atomically thin MoS_2 , causes a red-shift ≈ 70 meV for direct gap transition. On the other hand, Hui et.al, has reported the blue-shift of the direct band gap, photoluminescence and Raman active modes under the influence of external compressive strain. Similar, theoretical arguments have appeared justifying the role of strain in controlling the optical and electrical response of the MoS_2 Hui et al. (2013); Swastibrata Bhat-tacharyya (2014); Su et al. (2015); He et al. (2013b).

Hence, the observed blue-shift in samples S1 and S2 is due to strain in the samples whereas in sample S3 it is under the combined effect of compressive strain and quantum confinement effects.

Photoluminescence Spectroscopy

Fig.7 displays the photoluminescence spectra of different samples acquired using excitation wavelength of 320 nm. Bulk sample, displays a relatively weak and broad emission covering the range of C and D-type absorption. Other samples also display similar spectral features except that they are blue-shifted w.r.t. the bulk spectra. Therefore, as the strain has increased, the emission peaks in the PL spectra shifted to higher energy.

Conclusion

Different samples of MoS_2 were prepared using high energy ball-milling followed by probe-sonication in DMF. The diffraction peaks corresponding to various planes were shifted towards higher 2θ values, implying the presence of

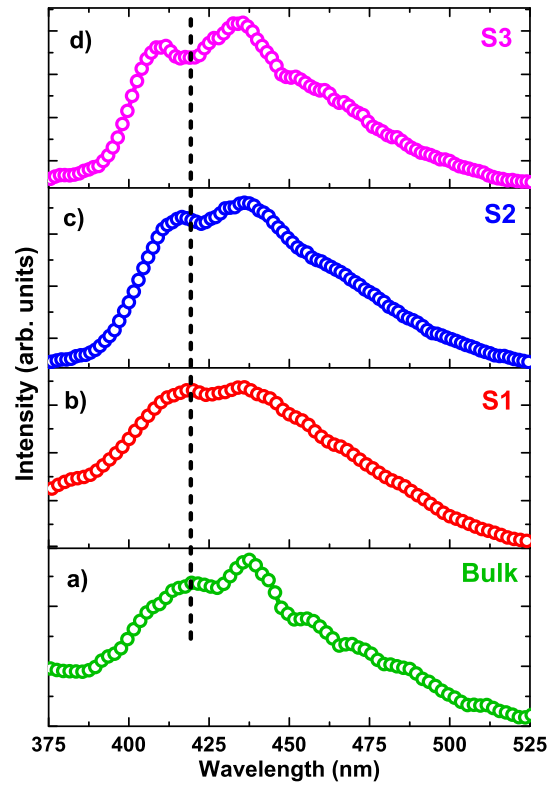


Figure 7: (color online) Photoluminescence spectra from MoS_2 nanostructures at 320 nm excitation wavelength for (a) Bulk crystalline powder (b) Ball Milled powder (c) probe sonicated powder and (d) probe sonicated suspension

compressive strain in ball-milled and sonicated samples. The maximum strain is observed in sample S3, which was obtained using ball-milling followed by probe sonication. The absorption spectra indicated the presence of various excitonic features, that are blue-shifted w.r.t the bulk sample. This is further corroborated by the blue-shift in the PL emission and in the characteristic, E_{2g}^1 and A_{1g} Raman modes. The observed blue-shift in powdered samples cannot be associated with quantum confinement effect as their size is quite away from the confinement regime. Therefore, we conclude that the compressive strain is responsible for the observed blue-shift in the absorption/emission and Raman modes. However, the possibility of quantum confinement cannot be excluded in MoS_2 nanosheets, where the sheet size in nano regime is also obtained. Thus, we conclude that strain engineering offers a new route to tune the structural as well as optical properties of material. And this is not only limited to optical but other physical properties like magnetism Zhou et al. (2012); Pan & Zhang (2012) can also be influenced by tunable strain.

Acknowledgment

One of the authors Shubham Bhagat acknowledges the GNDU-Amritsar, India for providing the fellowship under UPE-Scheme for carrying out her PhD work. The authors gratefully acknowledge UGC- New Delhi for providing financial assistance under the project No.F.30-137/2015(BSR).

References

References

- A R Beal, W. Y. L. (1976). Excitons in $2\text{H} - \text{WSe}_2$, $3\text{R} - \text{WS}_2$. *Journal of Physics C: Solid State Physics*, 9, 2459.
- Alidoust, N., Bian, G., Xu, S.-Y., Sankar, R., Neupane, M., Liu, C., Belopolski, I., Qu, D.-X., Denlinger, J. D., Chou, F.-C., & Hasan, M. Z. (2014). Observation of monolayer valence band spin-orbit effect and induced quantum well states in MoX_2 . *Nature Communications*, 5, 4673-.

- Allen, M. J., Tung, V. C., & Kaner, R. B. (2010). Honeycomb carbon: A review of graphene. *Chemical Reviews*, *110*, 132–145. PMID: 19610631.
- Bagnall, A., Liang, W., Marseglia, E., & Welber, B. (1980). Raman studies of MoS₂ at high pressure. *Physica B+C*, *99*, 343 – 346.
- Bhattacharyya, S., Pandey, T., & Singh, A. K. (2014). Effect of strain on electronic and thermoelectric properties of few layers to bulk MoS₂. *Nanotechnology*, *25*, 465701.
- Böker, T., Severin, R., Müller, A., Janowitz, C., Manzke, R., Voß, D., Krüger, P., Mazur, A., & Pollmann, J. (2001). Band structure of MoS₂, MoSe₂ and α -mote₂ : angle-resolved photoelectron spectroscopy and ab initio calculations. *Phys. Rev. B*, *64*, 235305.
- Bromley, R. A., Murray, R. B., & Yoffe, A. D. (1972). The band structures of some transition metal dichalcogenides. iii. group vi a: trigonal prism materials. *Journal of Physics C: Solid State Physics*, *5*, 759.
- Castro Neto, A. H., Guinea, F., Peres, N. M. R., Novoselov, K. S., & Geim, A. K. (2009). The electronic properties of graphene. *Rev. Mod. Phys.*, *81*, 109–162.
- Choi, W., Lahiri, I., Seelaboyina, R., & Kang, Y. S. (2010). Synthesis of graphene and its applications: A review. *Critical Reviews in Solid State and Materials Sciences*, *35*, 52–71.
- Eknapakul, T., King, P., Asakawa, M., Buaphet, P., He, R., Mo, S., Takagi, H., Shen, K., Baumberger, F., Sasagawa, T., Jungthawan, S., & Meevasana, W. (2014). Electronic structure of a quasi-freestanding MoS₂ monolayer. *Nano Letters*, *14*, 1312–1316.
- Gan, Z. X., Liu, L. Z., Wu, H. Y., Hao, Y. L., Shan, Y., Wu, X. L., & Chu, P. K. (2015). Quantum confinement effects across two-dimensional planes in MoS₂ quantum dots. *Applied Physics Letters*, *106*, 233113.

- Gopalakrishnan, D., Damien, D., & Shaijumon, M. M. (2014). MoS₂ quantum dot-interspersed exfoliated MoS₂ nanosheets. *ACS Nano*, *8*, 5297–5303. PMID: 24773177.
- He, K., Poole, C., Mak, K. F., & Shan, J. (2013a). Experimental demonstration of continuous electronic structure tuning via strain in atomically thin MoS₂. *Nano Letters*, *13*, 2931–2936.
- He, K., Poole, C., Mak, K. F., & Shan, J. (2013b). Experimental demonstration of continuous electronic structure tuning via strain in atomically thin MoS₂. *Nano Letters*, *13*, 2931–2936.
- Huang, M., Yan, H., Heinz, T. F., & Hone, J. (2010). Probing strain-induced electronic structure change in graphene by raman spectroscopy. *Nano Letters*, *10*, 4074–4079. PMID: 20735024.
- Hui, Y. Y., Liu, X., Jie, W., Chan, N. Y., Hao, J., Hsu, Y.-T., Li, L.-J., Guo, W., & Lau, S. P. (2013). Exceptional tunability of band energy in a compressively strained trilayer MoS₂ sheet. *ACS Nano*, *7*, 7126–7131.
- Jin, W., Yeh, P. C., Zaki, N., Zhang, D., Sadowski, J. T., Al-Mahboob, A., Van Der Zande, A. M., Chenet, D. A., Dadap, J. I., Herman, I. P., Sutter, P., Hone, J., & Osgood, R. M. (2013). Direct measurement of the thickness-dependent electronic band structure of MoS₂ using angle-resolved photoemission spectroscopy. *Physical Review Letters*, *111*.
- Kim, K. S., Zhao, Y., Jang, H., Lee, S. Y., Kim, J. M., Kim, K. S., Ahn, J.-H., Kim, P., Choi, J.-Y., & Hong, B. H. (2009). Large-scale pattern growth of graphene films for stretchable transparent electrodes. *Nature*, *457*, 706–.
- Kin Fai Mak, J. S. (2016). Photonics and optoelectronics of 2d semiconductor transition metal dichalcogenides. *Nature Photonics*, *10*, 216.
- Klein, A., Tiefenbacher, S., Eyert, V., Pettenkofer, C., & Jaegermann, W. (2001). Electronic band structure of single-crystal and single-layer WS₂: Influence of interlayer van der waals interactions. *Phys. Rev. B*, *64*, 205416.

- Latzke, D., Zhang, W., Suslu, A., Chang, T., Lin, H., Jeng, H., Tongay, S., Wu, J., Bansil, A., & Lanzara, A. (2015). Electronic structure, spin-orbit coupling, and interlayer interaction in bulk MoS₂ and WS₂, . *91*, 235202.
- Lee, C., Wei, X., Kysar, J. W., & Hone, J. (2008). Measurement of the elastic properties and intrinsic strength of monolayer graphene. *Science*, *321*, 385–388.
- Lu, P., Wu, X., Guo, W., & Zeng, X. C. (2012). Strain-dependent electronic and magnetic properties of MoS₂ monolayer, bilayer, nanoribbons and nanotubes. *Phys. Chem. Chem. Phys.*, *14*, 13035–13040.
- Molina-Sanchez, A., Sangalli, D., Hummer, K., Marini, A., & Wirtz, L. (2013). Effect of spin-orbit interaction on the optical spectra of single-layer, double-layer, and bulk mos₂. *Phys. Rev. B*, *88*, 045412.
- Mukherjee, S., Maiti, R., Midya, A., Das, S., & Ray, S. K. (2015). Tunable direct bandgap optical transitions in MoS₂ nanocrystals for photonic devices. *ACS Photonics*, *2*, 760–768.
- Murphy, A. (2007). Band-gap determination from diffuse reflectance measurements of semiconductor films, and application to photoelectrochemical water-splitting. *Solar Energy Materials and Solar Cells*, *91*, 1326 – 1337.
- Ni, Z. H., Yu, T., Lu, Y. H., Wang, Y. Y., Feng, Y. P., & Shen, Z. X. (2008). Uniaxial strain on graphene: Raman spectroscopy study and band-gap opening. *ACS Nano*, *2*, 2301–2305. PMID: 19206396.
- Novoselov, K. S. (2011). Nobel lecture: Graphene: Materials in the flatland. *Rev. Mod. Phys.*, *83*, 837–849.
- Padilha, J., Peelaers, H., Janotti, A., & Van de Walle, C. (2014). Nature and evolution of the band-edge states in MoS₂: From monolayer to bulk. *PhysRevB*, *90*, 205420.

- Pan, H., & Zhang, Y.-W. (2012). Tuning the electronic and magnetic properties of MoS₂ nanoribbons by strain engineering. *The Journal of Physical Chemistry C*, *116*, 11752–11757.
- Plechinger, G., Heydrich, S., Eroms, J., Weiss, D., Schller, C., & Korn, T. (2012). Raman spectroscopy of the interlayer shear mode in few-layer MoS₂ flakes. *Applied Physics Letters*, *101*, 101906.
- RosendoLpez, R. (2012). Band-gap energy estimation from diffuse reflectance measurements on sol–gel and commercial TiO₂ : a comparative study. *Journal of Sol-Gel Science and Technology*, *61*, 1–7.
- Sharma, S., Bhagat, S., Singh, J., Singh, R. C., & Sharma, S. (2017). Excitation-dependent photoluminescence from WS₂ nanostructures synthesized via top-down approach. *Journal of Materials Science*, *52*, 11326–11336.
- Sinha, A. K., Gupta, R. K., & Deb, S. K. (2012). A correlation between structural and optical properties of cobalt oxide nanoparticles for various annealing conditions. *Applied Physics A*, *108*, 607–613.
- Su, W., Dou, H., Li, J., Huo, D., Dai, N., & Yang, L. (2015). Tuning photoluminescence of single-layer MoS₂ using H₂O₂. *RSC Adv.*, *5*, 82924–82929.
- Suzuki, R., Sakano, M., Zhang, Y. J., Akashi, R., Morikawa, D., Harasawa, A., Yaji, K., Kuroda, K., Miyamoto, K., Okuda, T., Ishizaka, K., Arita, R., & Iwasa, Y. (2014). Valley-dependent spin polarization in bulk MoS₂ with broken inversion symmetry. *Nature Nanotechnology*, *9*, 611–.
- Swastibrata Bhattacharyya, A. K. S., Tribhuwan Pandey (2014). Effect of strain on electronic and thermoelectric properties of few layers to bulk MoS₂. *Nanotechnology*, *25*, 465701.
- Trainer, D. J., Putilov, A. V., Di Giorgio, C., Saari, T., Wang, B., Wolak, M., Chandrasena, R. U., Lane, C., Chang, T.-R., Jeng, H.-T., Lin, H., Kronast, F., Gray, A. X., Xi, X., Nieminen, J., Bansil, A., & Iavarone, M. (2017).

- Inter-layer coupling induced valence band edge shift in mono to few-layer MoS_2 . *Scientific Reports*, *7*, 40559.
- Virsek, M., Jesih, A., Milosevic, I., & Milan Damnjanovic, M. R. (2007). Raman scattering of the MoS_2 and WS_2 single nanotubes. *Surface Science*, *601*, 2868 – 2872.
- Wang, Q. H., Kalantar-Zadeh, K., Kis, A., Coleman, J. N., & Strano, M. S. (2012). Electronics and optoelectronics of two-dimensional transition metal dichalcogenides. *Nat Nano*, *7*, 699–712.
- Wilcoxon, J. P., Newcomer, P. P., & Samara, G. A. (1997). Synthesis and optical properties of MoS_2 and isomorphous nanoclusters in the quantum confinement regime. *Journal of Applied Physics*, *81*, 7934–7944.
- Wilcoxon, J. P., & Samara, G. A. (1995). Strong quantum-size effects in a layered semiconductor: MoS_2 nanoclusters. *Phys. Rev. B*, *51*, 7299–7302.
- Wilson, J., & Yoffe, A. (1969). The transition metal dichalcogenides discussion and interpretation of the observed optical, electrical and structural properties. *Advances in Physics*, *18*, 193–335.
- Wood, B. (1979). Diffuse reflectance spectra and optical properties of some sulphides and related minerals. *Mineralogical Magazine*, *43*, 509–518.
- Zhou, Y., Wang, Z., Yang, P., Zu, X., Yang, L., Sun, X., & Gao, F. (2012). Tensile strain switched ferromagnetism in layered NbS_2 and NbSe_2 . *ACS Nano*, *6*, 9727–9736. PMID: 23057936.
- Zhu, Z. Y., Cheng, Y. C., & Schwingenschlögl, U. (2011). Giant spin-orbit-induced spin splitting in two-dimensional transition-metal dichalcogenide semiconductors. *Phys. Rev. B*, *84*, 153402.